Kinetic Evidence for Interaction of Human Immunodeficiency Virus Type 1 Reverse Transcriptase with the 3′-OH of the Incoming dTTP Substrate†

Varuni K. Jamburuthugoda,‡ Dongdong Guo,§ Joseph E. Wedekind,‡ and Baek Kim*,§

Department of Microbiology and Immunology and Department of Biochemistry and Biophysics, University of Rochester, 601 Elmwood Avenue, Box 672, Rochester, New York 14642

Received April 1, 2005; Revised Manuscript Received May 24, 2005

ABSTRACT: Two previously identified human immunodeficiency virus type 1 (HIV-1) reverse transcriptase (RT) mutants, Q151N and V148I, are known to have reduced dNTP binding affinity but possess wild-type chemical catalysis rates. Structural modeling based on the crystal structure of the HIV-1 RT ternary complex with dTTP proposes that Q151N loses the interaction with the 3′-OH of the incoming dTTP and that V148I disrupts positioning of Q151 for this interaction. On the basis of this, we predicted that while wild-type (WT) HIV-1 RT would have decreased binding affinity to dTTP analogues lacking 3′-OH, compared to dTTP, the Q151N and V148I RT mutants should have decreased but similar affinity to both dTTP and dTTP analogues. Pre-steady-state kinetics on WT RT showed 14- and 53-fold higher K_d values for the 3′-OH lacking ddTTP and acyTTP, compared to dTTP. In contrast, the Q151N and V148I mutants, which were predicted to have lost H-bonding interaction with the 3′-OH of dTTP, showed higher but similar K_d values for dTTP, ddTTP, and acyTTP. Interestingly, the Q151N and V148I RTs bound to AZTTP approximately 12 and 18 times more tightly than to dTTP, respectively. Our structure modeling suggests that these RT mutants can interact with the azido moiety of AZTTP, which is 1.4 Å longer than the 3′-OH of dTTP. The kinetic data presented in this report demonstrate the functional role of the Q151 residue in HIV-1 RT interaction with dTTP and its analogues containing chemical modifications at the 3′-C of the sugar moiety.

Enzymatic incorporation of dideoxyribonucleotide chain terminators during DNA polymerization has been studied extensively with many different DNA polymerases due to the efficacy of these compounds. Historically, dideoxynucleotide triphosphate (ddNTP) incorporation by DNA polymerases played a central methodological role in decoding DNA sequences and the genetic content of specific genes (*1*, *2*). Incorporation of nucleotide chain terminators by cellular DNA polymerases has also been employed as a means to control cellular DNA replication, especially in cells with an uncontrolled proliferation phenotype such as cancer cells (*3*, *4*). Finally, nucleoside chain terminators continue to be extensively employed to inhibit DNA synthesis in parasitic microorganisms such as viruses. A variety of new and effective antiviral DNA polymerase nucleoside chain terminators have been developed for the treatment of viral infections. The nucleoside reverse transcriptase (RT)[1] inhibitors (NRTIs), such as AZT, 3TC, D4T, ddC, and ddI, are major chemotherapeutic agents for the treatment of individuals infected with human immunodeficiency virus type 1 (HIV-1) (*5*, *6*). The cross-organism effectiveness of these NRTIs is highly beneficial for the treatment of infections by numerous viruses.

Mechanisms by which DNA polymerases distinguish between natural dNTP and ddNTP have been revealed by kinetic and structural analyses of both wild-type and mutant DNA polymerases. Pre-steady-state kinetic analysis, which can determine substrate binding affinity (K_d) and reaction rate (k_{pol}) under single turnover conditions, has been employed to understand the mechanisms by which various DNA polymerases distinguish ddNTPs from dNTPs (*7*, *8*). For example, the Klenow fragment (KF) of *Escherichia coli* DNA polymerase I, which can efficiently distinguish ddNTPs from dNTPs (selectivity = 5.7×10^3), discriminates against ddNTP during the k_{pol} step (conformational change/chemistry), especially the conformational change step (*7*). A similar case was observed in thermostable *Taq* polymerase (*2*). However, DNA polymerase α (RB69 DNA polymerase), which has very high selectivity against ddNTPs (7.3×10^4), discriminates against ddNTP in both K_d and k_{pol} steps (*9*). HIV-1 RT moderately differentiates ddNTP over dNTP (selectivity = ∼5) and uses both the K_d and k_{pol} steps for discrimination, even though the ddNTP selectivity value can vary depending on the nature of the substrates (i.e., sequences of T/P and kinds of ddNTPs) and types of assays (*10*−*13*). In contrast, human mitochondrial DNA polymerase γ (*14*),

† This work was supported by research grants AI49781 (to B.K.) and GM63162 (to J.E.W.) from the National Institutes of Health.

* Corresponding author. Tel: (585) 275-6916. Fax: (585) 473-9573. E-mail: baek_kim@urmc.rochester.edu.

‡ Department of Biochemistry and Biophysics, University of Rochester.

§ Department of Microbiology and Immunology, University of Rochester.

[1] Abbreviations: HIV-1, human immunodeficiency virus type 1; RT, reverse transcriptase; dTTP, 2′-deoxythymidine 5′-triphosphate; ddTTP, 2′,3′-dideoxythymidine 5′-triphosphate; acyTTP, 9-[(2-hydroxyethoxy)-methyl)]thymine triphosphate; AZTTP, 3′-azido-3′-deoxythymidine 5′-triphosphate; T/P, template-primer complex; p66, 66 kDa HIV-1 RT polypeptide; SDS, sodium dodecyl sulfate.

10.1021/bi050611+ CCC: $30.25
Published on Web 07/14/2005

rat DNA polymerase β, and phage T7 DNA polymerase (exo-) (*13*) very poorly distinguish ddNTP and dNTP (selectivity = ~1) during single turnover reactions.

The analysis of the DNA polymerase mutants with altered capabilities in the dNTP/ddNTP discrimination is a cornerstone for understanding structural and mechanistic elements of the enzymatic discrimination between dNTP and ddNTP. For example, there is no direct interaction between KF and 3′-OH of dNTP during the substrate binding (K_d) step (*7*), which supports the absence of discrimination capability during the binding step. However, Phe762 of KF appears to induce a possible interaction with the 3′-OH of the incoming dNTP during the conformational change (*7*). Tyr substituted at this position could donate its own OH during the conformational change when ddNTP, which lacks a 3′-OH, occupies the dNTP binding site of KF. This would enable the Tyr mutant to incorporate ddNTP, making it less efficient at discriminating ddNTP over dNTP. A possible model for the KF interaction with the 3′-OH of dNTP during the conformational change proposed that Glu710 of KF may interact with Mg^{2+} which can interact with the 3′-OH of dNTP (*7*). This indirect interaction with the 3′-OH of dNTP was supported by the reduced ddNTP/dNTP discrimination capability of the E710A mutant and the Mg^{2+} dependence of ddNTP incorporation (*7*).

Interestingly, the structure of the HIV-1 RT−template/primer (T/P)−dTTP ternary complex demonstrated that the 3′-OH of dTTP projects toward a small pocket consisting of a series of RT residues including Asp113, Tyr115, Phe116, and Gln151 and the peptide backbone between residues 113 and 115 (*15*). In this ternary complex, the side chain of Q151 appears to directly interact with the 3′-OH of dTTP. Previously, we reported that the Q151N mutation greatly increases the K_d value of HIV-1 RT for dNTP, without affecting the k_{pol} value, indicating an interaction between Q151 and the incoming dNTP during the formation of the ternary complex (*16*, *17*). The V148I mutation, which was originally identified in an in vivo RT variant (*18*), also showed the same K_d and k_{pol} alterations as the Q151N mutation (*19*). We proposed that the V148I mutation, with a longer side chain than the wild-type valine, may move the nearby Q151 residue away from the active site, resulting in the interference of the interaction between Q151 and the 3′-OH of dNTP (*19*). We recently reported that pseudotyped HIV-1 variants containing these dNTP binding RT mutants failed to infect human macrophages containing low cellular dNTP concentrations (~40 nM) even though these viruses efficiently infect activated/dividing CD4+ T cells containing approximately 100-fold higher cellular dNTP concentration (2−5 μM) (*20*). This result suggested that the binding affinity of HIV-1 RT for the dNTP substrate contributes to the cell-type specificity of HIV-1 that is closely related with HIV pathogenesis. In addition, the Q151N and V148I HIV-1 RT mutants also show a 13- and 8.7-fold higher enzymatic fidelity than wild-type RT, respectively (*16*, *21*). Our kinetic analysis demonstrated that the reduced mismatch extension fidelity is responsible for the fidelity increase by both Q151N and V148I mutation (*16*). Consistent with this, HIV-1 mutant viruses containing Q151N or V148I RTs show decreased viral genomic mutagenesis (*16*).

In this study, we kinetically tested a structural model in which the Q151 residue of HIV-1 RT interacts with the 3′-OH of the incoming dTTP. This model predicts that, unlike wild-type HIV-1 RT, the Q151N and V148I mutants, which have lost the interaction with the 3′-OH of the dTTP substrate, should show similar binding affinity to both natural dTTP and nucleotide analogues lacking 3′-OH. The pre-steady-state data of wild type and the Q151N and V148I mutants with nucleotide analogues support the interaction between Q151 and the 3′-OH of the dTTP substrate.

MATERIALS AND METHODS

Purification of HIV-1 RT Proteins. HIV-1 RT proteins, wild type, Q151N, and V148I, were overexpressed in *E. coli* BL21 (Novagen, Madison, WI) from derivatives of the pET28a-HIV-1 RT plasmid (HXB2). The HIV-1 RT expression construct encodes full-length HIV-1 RT (HXB2) fused at the N terminus to a six-histidine tag. The hexahistidine-tagged RT was purified using Ni^{2+} chelation chromatography as described previously (*21*−*23*). From 1 L of culture, we were able to purify 4 mg of p66 homodimers. To examine the purity of the purified RT proteins, 4 μg of the purified RTs was analyzed by 10% SDS−polyacrylamide gels using 4 μg of 98% pure bovine serum albumin (BSA) (Sigma-Aldrich, St. Louis, MO) as a control. The gels visualized by Coomassie staining were analyzed by a densitometer, and the purified RT proteins showed similar levels of minor contaminants as the BSA control, suggesting that the RT proteins used in this study must be at least 95% pure. Four different nucleotides were used in this study: dTTP (USB, City, OH), ddTTP (Amersham Biosciences Corp., City, NJ), acyTTP (New England Biolabs, City, MA), and AZTTP (Moravek Biochemical, City, CA). DNA primers (Integrated DNA Technologies, Ames, IA) were labeled with [γ-^{32}P]-ATP (Amersham Biosciences Corp).

Molecular Dynamics. To assess the packing effects of the Q151N and V148I mutations (Figure 1), the crystal structure of RT (*15*) was altered to include the respective amino acid changes. Mutations were introduced using the interactive graphics program O (*24*) and an appropriate side-chain rotamer was assigned from the accompanying database. Hydrogen atoms were assigned to each set of coordinates in CNS (*25*), and the structures were subjected to 0.50 ps of molecular dynamics (0.0005 ps steps) at 298 K. The positions of dTTP, Mg (II), and DNA were harmonically restrained throughout the simulation. Coordinates for AZTTP were obtained from ref *33*. The AZTTP molecule was manually positioned on dTTP derived from the crystal structure of RT (*15*) using the wild-type or mutant structures as starting models (Figure 6). Each model was subsequently subjected to molecular dynamics as described. The resulting models were each inspected for potential hydrogen bond networks, and manual adjustments were made in the amino acid side chains of Q151 and N151 to optimize potential interactions.

Pre-Steady-State Kinetic Assays. Pre-steady-state burst and single turnover experiments were performed to examine the transient kinetics associated with incorporating a single nucleotide onto the T/P. To study the incorporation of each of the four different types of nucleotide, a ^{32}P-labeled 23-mer primer (T primer, 5′-CCGAATTCCCGCTAGCAATAT-TC-3′; Integrated DNA Technologies) was annealed to a 38-mer RNA template (5′-GCUUGGCUGCAGAAUAUUG-CUAGCGGGAAUUCGGCGCG-3′; Dharmacon Research,

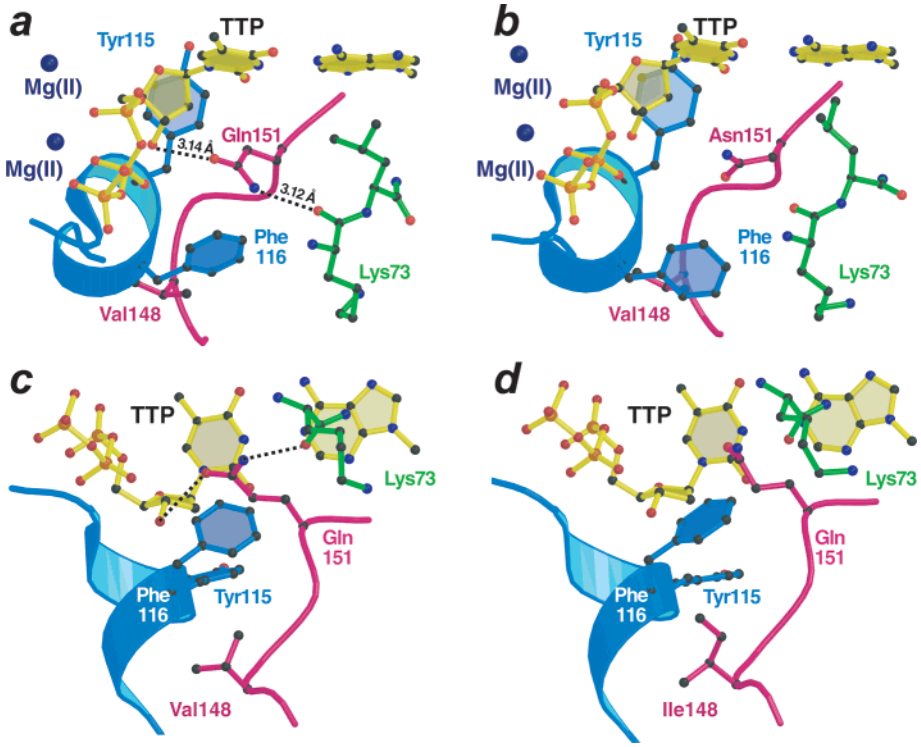

FIGURE 1: Schematic diagrams of the RT active site bound to dTTP and T/P based on the crystal structure solved by Huang et al. (*15*). (a) The native RT active site showing key amino acids and nucleotides as ball-and-stick models. Hydrogen bond distances to Gln151 were derived from the better ordered structure in the asymmetric unit defined by ref *15*. (b) The Q151N mutant conformation resulting from molecular dynamics simulations. Key hydrogen bond interactions to the amide side chain of Asn151 cannot be made as a result of the mutation. (c) View of the native RT structure rotated 90° about the *x*-axis relative to (a). Atom Cγ1 of Val148 packs against atom Cβ of Phe116 with a distance of 4.3 Å. (d) Conformation of the V148I mutant resulting from molecular dynamics. The side-chain rotamer adopted by Ile148 is necessary to prevent close contacts elsewhere in this hydrophobic pocket. Atom Cδ1 of Ile148 packs against atom Cβ of Phe116 with a distance of 4.4 Å; however, Gln151 must shift to accommodate this interaction.

Chicago, IL). Reactions were performed using a Kintek rapid quench machine (*17*, *26*, *27*). Products were analyzed by 14% denaturing sequencing gel electrophoresis and quantified with the Cyclone PhosphorImager (Perkin-Elmer Life Sciences, Boston, MA). Pre-steady-state burst experiments were employed to determine the active site concentrations of the HIV-1 RT proteins on the T/P. In this experiment, 800 μM dTTP was rapidly mixed with RT (150 nM RTs) prebound onto T/P (300 nM). In the pre-steady-state single turnover experiments that measured the dNTP concentration dependence of the purified RT protein, excess active RT (200 nM) (as determined by the burst experiments) was added to T/P (50 nM).

Data Analysis. Pre-steady-state kinetic data were analyzed using nonlinear regression. Equations were generated with the program KaleidaGraph version 3.51 (Synergy Software, Essex Junction, VT). Data points obtained during the burst experiment were fit to the burst equation:

$$[\text{product}] = A[1 - \exp(-k_{obs}t) + k_{ss}t] \qquad (1)$$

(*26*, *28*). The value A is the amplitude of the burst, which reflects the actual concentration of enzyme that is in active form. k_{obs} is the observed first-order rate constant for dNTP incorporation whereas k_{ss} is the observed steady-state rate constant (*26*, *27*, *29*). Data from single turnover experiments were fit to a single exponential equation that measures the rate of dNTP incorporation (k_{obs}) per given dNTP concentration [dNTP]. These results were then used to determine K_d, the dissociation constant for dNTP binding to the RT-T/P binary complex, and k_{pol}, the maximum rate of chemical catalysis/conformational change. This was done by fitting the data to the hyperbolic equation:

$$k_{obs} = k_{pol}[\text{dNTP}]/(K_d + [\text{dNTP}]) \qquad (2)$$

From this equation, we could then identify the kinetic constants for each RT during pre-steady-state kinetics: k_{pol}, the maximum rate of dNTP incorporation, and K_d, equilibrium dissociation constant for the interaction of dNTP with the E·DNA complex (*26*, *30*).

RESULTS

Modeling of the Two dNTP Binding Mutants of HIV-1 RT, Q151N and V148I. We previously characterized two HIV-1 RT mutants, Q151N and V148I, that have reduced dNTP binding affinity. These mutations increased the K_d value without affecting the k_{pol} value. A structural and computational analysis of each mutant, compared to native RT, provided a possible explanation for the apparent loss of dNTP affinity (Figure 1). In the crystal structure of the HIV-1 RT ternary complex (RT−T/P−dTTP) (*15*), the amide side chain of Q151 accepts a hydrogen bond to its amide oxygen from the 3′-OH of dTTP, whereas the amide NH_2 of the side chain donates a hydrogen bond to the backbone carbonyl oxygen of K73 (Figure 1a). A molecular dynamics simulation of the Q151N mutation indicated that the shorter side chain of Asn is incapable of commensurate interactions with the dTTP and protein moieties as the Gln (Figure 1b). In the Q151N model, the distance between the amide group of the N151

side chain and the 3′-OH of dTTP is ~4.5 Å (in contrast to 3.14 Å for Q151), which precludes the possibility of hydrogen bond formation. Consequently, the active site is somewhat "looser", as reflected by motions in the side chains of F116 and K73 (Figure 1a,b). Failure of the Q151N mutant to interact with the 3′-OH of dTTP in the model corroborates the reduction of the dNTP binding affinity observed in our pre-steady-state analysis of Q151N and provides a molecular explanation for this phenomenon.

In the active site of the HIV-1 RT ternary complex, V148 does not interact directly with substrates (Figure 1a,c). However, the V148 resides at the carboxylic end of a short helical element whose side chains of Y115 and F116 form an integral part of the active site as manifested through van der Waals contacts to dTTP and Q151, respectively (Figure 1c). Molecular dynamics simulations on the V148I mutant revealed the importance of the latter aromatic residues in maintaining the correct conformation of Q151. Specifically, I148 adopts a new side-chain rotamer that disrupts the F116 side chain by pushing it closer to dTTP (Figure 1c,d) in order to accommodate an extra methyl group from the V to I change. In the native RT structure, F116 was already close to the side chain of Q151 (~3.1 Å between the amide nitrogen and Cϵ2 of the aromatic ring). Hence, incidental contact between I148 and F116 causes steric clouding leading to direct disruption of the hydrogen bonds of Q151. The inability of the amide group to engage in its normal hydrogen-bonding pattern could result in a nonproductive interaction similar to that found in Q151N that prevents binding to dTTP. This observation also supports our observed reduction of the RT binding affinity to the incoming dTTP substrate as manifested by the higher K_d.

In this study, we further examined the interaction of the Q151 residue with the 3′-OH of the incoming dNTP substrate by testing a prediction made by the structure-based modeling (Figure 1). Notably, wild-type RT may have poorer binding affinity to ddNTP than dNTP due to the absence of enzyme interactions with the 3′-OH of ddNTP. Similarly, the Q151N and V148I HIV-1 RT mutants should exhibit comparably poor but similar affinity to both dNTP and ddNTP caused by loss of productive interactions with the 3′-OH of substrate due to the respective mutations. Basically, unlike wild-type RT, the nucleotide substrate binding of the two RT mutants is likely not affected by the removal of the 3′-OH of the dNTP substrate. For this test, we determined binding affinity (K_d) and reaction rate (k_{pol}) of the wild-type and two mutant RTs with dTTP and three dTTP analogues containing various chemical modifications at the 3′ position: ddTTP, acyTTP, and AZTTP (Figure 2). We chose dTTP and its analogues because the available structure for the HIV-1 RT ternary complex was obtained with dTTP (*15*). ddTTP does not possess the 3′-OH group at it sugar moiety, and acyTTP has neither 3′-OH nor C3 due to the disrupted sugar structure. In contrast, AZTTP has an azido group, which is significantly longer than the OH group of dTTP.

Active Site Concentrations of HIV-1 RT Proteins. We first determined the active concentrations of three HIV-1 RT proteins, wild type, Q151N, and V148I, on a ^{32}P-labeled 23-mer (T primer) annealed to a 38-mer RNA template (T primer/template) as described previously (*16*). We measured product formation when 800 μM dTTP was mixed with RT (150 nM as determined with a Bradford assay), prebound

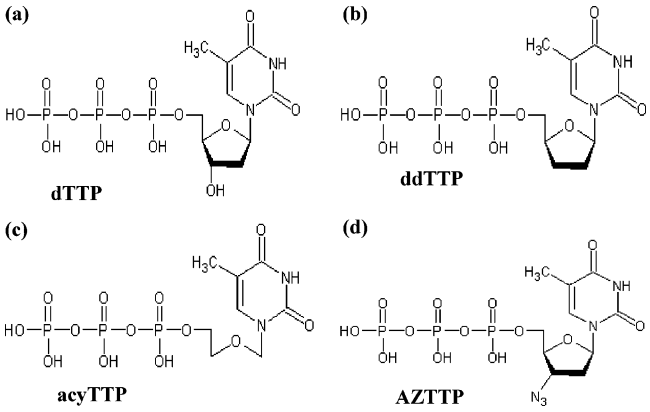

FIGURE 2: Structures of (a) dTTP, (b) ddTTP, (c) acyTTP, and (d) AZTTP.

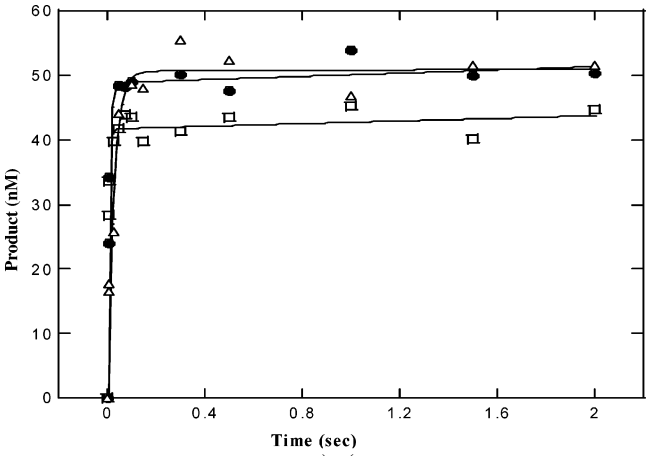

FIGURE 3: Active site titration of HIV-1 RT WT, Q151N, and V148I. Pre-steady-state and steady-state kinetics of HIV-1 RT WT (●), Q151N (△), and V148I (□) incorporating correct dTTP onto the ^{32}P-labeled 23-mer T primer annealed to the 38-mer RNA template were analyzed. Reactions were carried out at the indicated times by mixing together prebound RT (150 nM)·T/P (300 nM) with 800 μM dTTP under rapid quench conditions (see Materials and Methods). The data were fit into the burst equation (eq 1; see Materials and Methods) as indicated by the solid line, which provides a measure of the active concentration of RT (Amp), the observed first-order rate constant for the burst phase (k_{obs}), and the first-order rate constant for the linear phase (k_{ss}) for WT, Q151N, and V148I HIV-1 RT. The active concentration (Amp) of WT was 48.9 ± 4.7 nM. Its k_{obs} was 128.5 ± 10 s^{-1}, and its k_{ss} was 4.1 × 10^{-2} ± 2.6 × 10^{-2} s^{-1}. The active site concentration of Q151N was 50.65 ± 2.4 nM. Its k_{obs} was 37.75 ± 6 s^{-1}, and its k_{ss} was 3.7 × 10^{-2} ± 1.2 × 10^{-2} s^{-1}. The active concentration (Amp) of V148I was 41.6 ± 4.7 nM. Its k_{obs} was 200 ± 24 s^{-1}, and its k_{ss} was 2.4 × 10^{-2} ± 1.8 × 10^{-2} s^{-1}.

onto the T/P (300 nM: excess T/P). There is an initial burst of product formation due to dTTP incorporation onto the prebound RT·T/P complex (pre-steady-state kinetics), which is followed by a slower and linear phase of product formation corresponding to the steady-state kinetics associated with multiple rounds of DNA polymerization (Figure 3). By fitting these results to eq 1 (see Materials and Methods), we see that the active site concentrations of wild-type, Q151N, and V148I HIV-1 RT proteins were all approximately 30−40%. Additional data obtained from these burst experiments include measurements for the rates of DNA polymerization during the pre-steady-state (k_{obs}) and steady-state (k_{ss}). The pre-steady-state rates of dTTP incorporation onto the T/P (k_{obs}) for the wild-type, Q151N, and V148I RT were 128.5

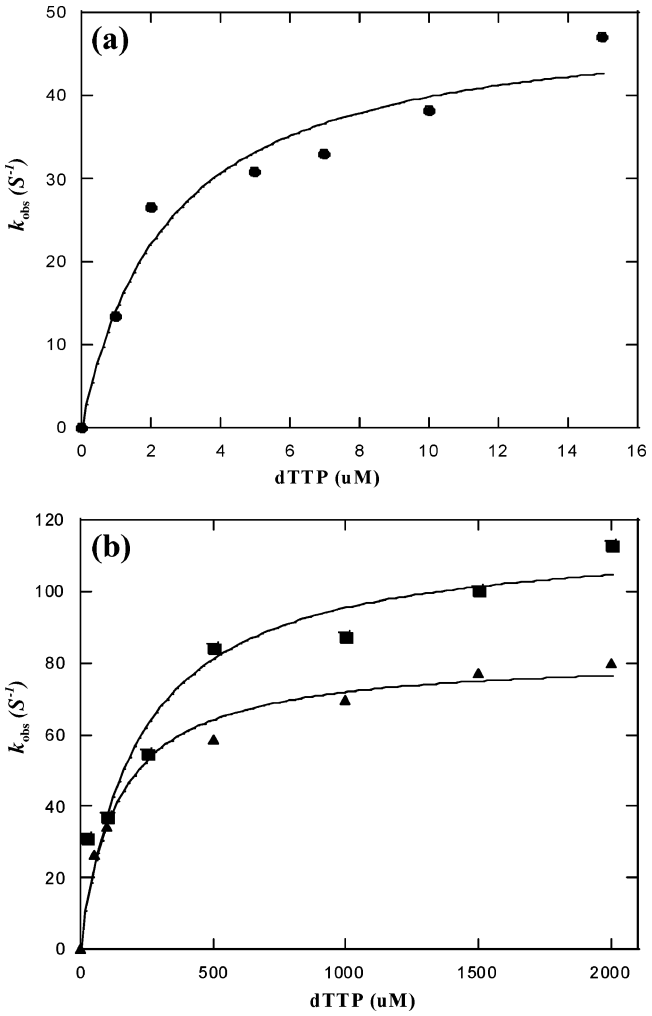

FIGURE 4: Pre-steady-state kinetics of dTTP incorporation by (a) WT and (b) Q151N (▲) and V148I (■) HIV-1 RTs. The ^{32}P-labeled 23-mer T primer annealed to the 38-mer RNA template (50 nM) was extended with excess RT (200 nM) for the single round dTTP incorporation at six different dTTP concentrations. The k_{obs} value at each dTTP concentration was plotted, and the k_{pol} and K_d values of each RT protein were fit into eq 2 as indicated by the solid line. The data for dTTP were summarized in Table 1.

$\pm$ 10, 37.75 $\pm$ 6, and 200 $\pm$ 24 s^{-1}, respectively, and their rates during the steady state were $4.1 \times 10^{-2} \pm 2.6 \times 10^{-2}$, $3.7 \times 10^{-2} \pm 1.2 \times 10^{-2}$, and $2.4 \times 10^{-2} \pm 1.8 \times 10^{-2}$ s^{-1}, respectively.

K_d and k_{pol} Determination of HIV-1 RT Proteins with dTTP. Next, we performed single turnover experiments (200 nM active RT and 50 nM T/Ps) to obtain an actual measure for the dTTP incorporation rate at different dTTP concentrations during the pre steady state. By measuring reaction rate (k_{obs}) as a function of dTTP concentrations (Figure 4), we were able to measure the kinetic parameters K_d, or the binding affinity of RT to the incoming nucleotide substrate, and k_{pol}, the maximum rate of dNTP incorporation (conformational change and chemical catalysis). As shown in Table 1, the K_d values of wild-type, Q151N, and V148I HIV-1 RT proteins to dTTP are 2.5, 137.8, and 222 μM, respectively, while the respective k_{pol} values are 36.6, 81.7, and 117.5 s^{-1}. While the k_{pol} values of the two RT mutant proteins are similar to that of wild-type RT, their binding affinities to the incoming dTTP are 55- and 89-fold less than that of wild-type HIV-1 RT. These data indicate that the Q151N and V148I mutations reduce dTTP substrate binding affinity with little effect on the rate of conformational change and catalysis. Overall, these two RT proteins have 24.5- and 27.3-fold less dTTP incorporation efficiency (k_{pol}/K_d) than wild-type HIV-1 RT, respectively (Table 1).

Incorporation of ddTTP by HIV-1 RT Proteins. Next, we determined the pre-steady-state kinetic parameters of the wild-type, Q151N, and V148I HIV-1 RT mutants using ddTTP under the same reaction conditions as described for dTTP incorporation. As shown in Figure 5 and Table 1, wild-type HIV-1 RT showed 14-fold lower binding affinity to ddTTP than to dTTP. These data indicate that the 3′-OH of the incoming dTTP substrate contributes significantly to the overall tight dTTP substrate binding of wild-type HIV-1 RT during formation of the RT−dTTP−T/P ternary complex. However, unlike what was observed with dTTP, the K_d values of Q151N and V148I mutant RTs to ddTTP were 63.9 and 81.6 μM, which are similar to that of wild-type HIV-1 RT to ddTTP (35.6 μM). These data are consistent with the prediction by the structural model that the Q151N and V148I mutants show wild-type levels of binding affinity to ddTTP because, unlike dTTP, the binding of ddTTP is independent of the interaction with the side chain of Q151 as illustrated in Figure 1.

The k_{pol} values of wild-type RT for ddTTP were low, compared to those for dTTP (Table 1). Interestingly, the k_{pol} values of the two RT mutants for ddTTP were similar to that of wild-type RT for this substrate. Like wild-type RT, the two RT mutants also showed 7−16-fold lower k_{pol} values compared to those for dTTP. These data suggest that the removal of the 3′-OH at the sugar moiety of the substrate affects the k_{pol} step (conformational step/catalysis) equally for the three RT proteins. This equal k_{pol} effect could be due to the altered geometry of the triphosphates of the ddNTP. This alteration causes loss of interactions with the 3′-OH and the β-phosphate of the incoming dNTP as proposed in the studies with KF enzyme, using the k_{pol} step to discriminate ddNTP over dNTP (*7*).

Incorporation of acyTTP by HIV-1 RT Proteins. Next, we determined the pre-steady-state kinetic parameters of the three HIV-1 RT proteins (wild type, Q151N, and V148I) using another chain terminator, acyTTP, which lacks the 3′-OH due to the disrupted sugar ring structure (Figure 2). As shown in Table 2, wild-type HIV-1 RT displayed a 53-fold higher K_d for acyTTP than for dTTP. As expected, both Q151N and V148I mutants had high but comparable K_d values for acyTTP and dTTP. These K_d values for acyTTP were also similar with those measured for ddTTP (Table 1). Therefore, as described above for ddTTP, these data indicate that the binding of acyTTP is also independent of any interaction with residue Q151 and is unaffected by the Q151N and V148I mutations. This supports the prediction made from the model for the interaction between the Q151 residue of HIV-1 RT with the 3′-OH of dTTP substrate. Since the K_d value of wild- type RT with acyTTP is similar to that with ddTTP, it is likely that even though the chemical modifications contained in ddTTP and acyTTP are different, these modifications induce a similar net loss of substrate affinity to the RT active site. In addition, the k_{pol} value of wild-type RT (and two mutants) with acyTTP is also not significantly different from that with ddTTP, suggesting that the chemical modifications of these two different chain

Table 1: Pre-Steady-State Kinetic Parameters of HIV-1 RT WT, Q151N, and V148I with dTTP and ddTTP

		kinetic parameter (*x*-fold difference)[a,b]		
substrate	HIV-1 RT	K_d (μM)	k_{pol} (s^{-1})	k_{pol}/K_d ($\mu M^{-1} s^{-1}$)
dTTP	wild type[c]	2.50 ± 1.4 (1)	36.6 ± 7.5 (1)	14.46 (1)
	Q151N	137.8 ± 24.2 (55)[a]	81.7 ± 5.6 (2.23)[a]	0.59 (0.040)[a]
	V148I	222 ± 71.7 (89)[a]	117.5 ± 9.7 (3.21)[a]	0.53 (0.036)[a]
ddTTP	wild type	35.6 ± 11.6 (1) (14.2)[b]	5 ± 0.37 (1) (0.14)[b]	0.14 (1) (0.010)[b]
	Q151N	63.9 ± 9.59 (1.79)[a] (0.46)[b]	5 ± 0.23 (1)[a] (0.061)[b]	0.078 (0.55)[a] (0.132)[b]
	V148I	81.6 ± 10.6 (2.29)[a] (0.37)[b]	8 ± 0.28 (1.6)[a] (0.068)[b]	0.09 (0.64)[a] (0.170)[b]

[a] *x*-fold differences of mutant RTs relative to wild-type HIV-1 RT. [b] *x*-fold differences for each enzyme relative to dTTP. [c] Data previously published (*35*).

terminators appear to affect the k_{pol} step (conformational change/catalysis) of wild-type HIV-1 RT (and two RT mutants) to a similar extent (Table 2).

Incorporation of AZTTP by HIV-1 RT Proteins. Lastly, we further elaborated the model for the Q151 interaction with the 3′-OH of dTTP by analyzing the incorporation of AZTTP. In contrast to ddTTP and acyTTP lacking the 3′-OH group, AZTTP contains a bulky azido group at the C3 position (Figure 2), which is 1.43 Å longer than the 3′-OH group of dTTP. It is possible that the N151 mutant, which appears to not interact with the 3′-OH of natural dTTP substrate, may still be able to interact with the longer azido group of AZTTP. This possibility predicts that the Q151N mutant may have tighter binding affinity to AZTTP than to dTTP as well as ddTTP and acyTTP. Several pre-steady-state studies reported that wild-type HIV-1 RT binds to AZTTP as tightly as dTTP, which was also observed in this study (Table 2) (*29*, *31*). As shown in Table 2, the two mutant RTs showed lower binding affinity to AZTTP (5.2−5.7-fold) than wild type. However, the binding affinity of the Q151N and V148I mutant RTs to AZTTP is approximately 12−18 times higher than that to the natural dTTP substrate, which is consistent with the prediction. Therefore, the tighter binding of the mutant RTs to AZTTP, compared to dTTP, supports that the shorter side chain of N151 in Q151N and the repositioned Q151 in V148I are able to make significant contacts with the azido group of AZTTP, facilitating the AZTTP binding to the active site during the ternary complex formation. However, since wild-type RT showed approximately a 5-fold higher AZTTP binding affinity than the two RT mutants, it suggested that the AZTTP interaction with the Q151 residue of the wild-type RT is stronger than that of the shortened N151 mutant residue or the repositioned Q151 residue resulting from the V148I mutant.

DISCUSSION

The structure of the HIV-1 RT complexed with T/P and dTTP has identified many active site residues that interact with the dTTP substrate (*15*). Unlike many structurally known DNA polymerases such as KF of *E. coli* DNA polymerase I, HIV-1 RT uniquely possesses an active site residue, Q151, which directly interacts with the 3′-OH of the incoming nucleotide substrate (dTTP) (*15*, *21*). As illustrated in Figure 1, the amide side chain of Q151 of HIV-1 RT accepts a hydrogen bond to its amide oxygen from the 3′-OH of dTTP. Since the RT interaction with the 3′-OH of dTTP is detected in the ternary complex (RT−T/P−dTTP) and since the Q151N and V148I HIV-1 RT mutations, which result in loss of interaction with the 3′-OH of dTTP, reduced

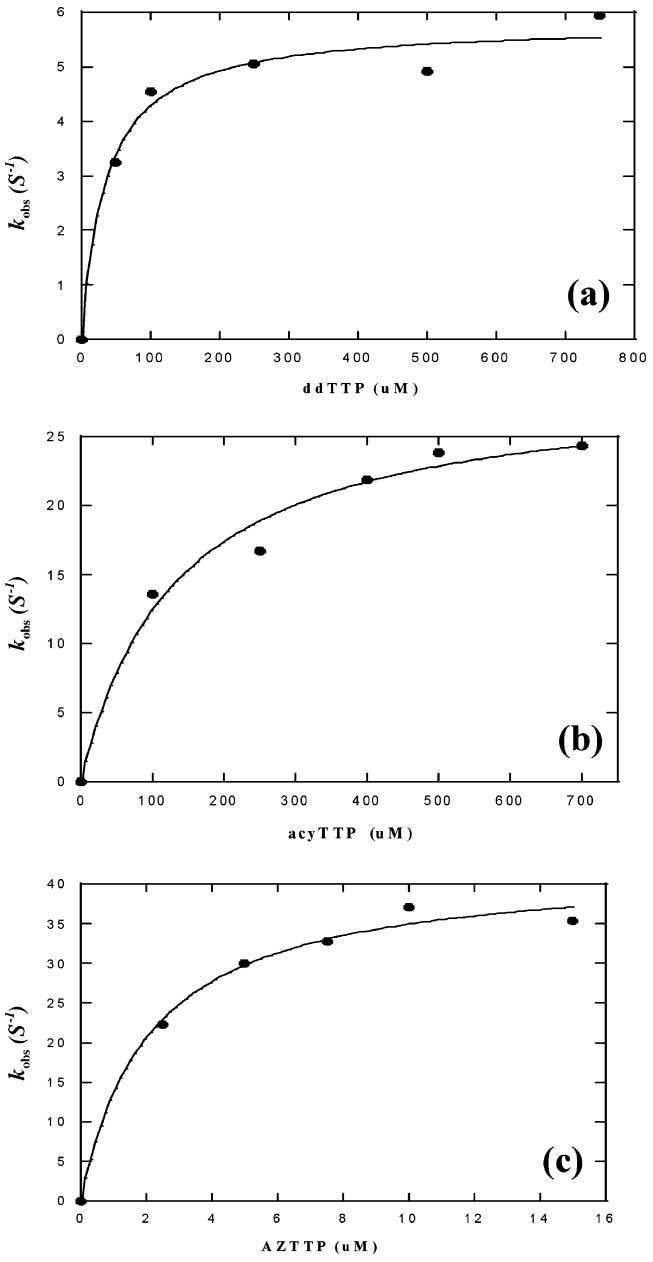

FIGURE 5: Pre-steady-state kinetics of (a) ddTTP, (b) acyTTP, and (c) AZTTP incorporation by WT HIV-1 RT. The ^{32}P-labeled 23-mer T primer annealed to the 38-mer RNA template (50 nM) was extended with excess RT (200 nM) for the single round ddTTP, acyTTP, and AZTTP incorporation at five different concentrations. The k_{obs} value at each dTTP analogue concentration was fit into eq 2 (see Materials and Methods) as indicated by the solid line to obtain k_{pol} and K_d values. The data for ddTTP were summarized in Table 1, and data for acyTTP and AZTTP were summarized in Table 2.

Table 2: Pre-Steady-State Kinetic Parameters of HIV-1 RT WT, Q151N, and V148I with acyTTP and AZTTP

		kinetic parameter (*x*-fold difference)[a,b]		
substrate	HIV-1 RT	K_d (μM)	k_{pol} (s^{-1})	k_{pol}/K_d ($\mu M^{-1} s^{-1}$)
acyTTP	wild type	132 ± 35 (1) (52.8)[b]	28 ± 2 (1) (0.77)[b]	0.21 (1) (0.01)[b]
	Q151N	70 ± 22 (0.53)[a] (0.51)[b]	22 ± 1.1 (0.78)[a] (0.27)[b]	0.31 (1.47)[a] (0.53)[b]
	V148I	72 ± 20 (0.54)[a] (0.32)[b]	9 ± 0.58 (0.32)[a] (0.08)[b]	0.12 (0.57)[a] (0.23)[b]
AZTTP	wild type	2.11 ± 0.42 (1) (0.84)[b]	42 ± 2 (1) (1.14)[b]	19.90 (1) (1.38)[b]
	Q151N	11.03 ± 5.6 (5.2)[a] (0.08)[b]	76.12 ± 18.2 (1.8)[a] (0.9)[b]	6.9 (0.34)[a] (11.7)[b]
	V148I	12.03 ± 4.51 (5.7)[a] (0.05)[b]	13.76 ± 1.7 (0.32)[a] (0.12)[b]	1.14 (0.05)[a] (2.2)[b]

[a] *x*-fold differences of mutant RTs relative to wild-type HIV-1 RT. [b] *x*-fold differences for each enzyme relative to dTTP (Table 1).

the K_d value for dTTP without affecting the k_{pol} value, it is likely that the hydrogen bond between the side chain of Q151 and the 3′-OH of dTTP contributes to the formation of the stable ternary complex from the binary complex (RT−T/P). More specifically, in the stepwise DNA polymerization reaction model, the entry of dTTP substrate into the active site of the binary complex can be facilitated by the interaction between Q151 and the 3′-OH of dTTP, leading to the formation of the open HIV-1 RT ternary complex (RT−T/P−dNTP). This form can now undergo a conformational change that closes the complex structure (RT*−T/P−dNTP), followed by fast chemical catalysis.

The structural observation of the direct interaction between the Q151 residue and the 3′-OH of dTTP, together with the kinetic data for the reduced K_d for Q151N and V148I mutation, predicts that, unlike wild-type RT, the Q151N and V148I, which cannot interact with the 3′-OH of dNTP, likely have reduced but similar binding affinities (K_d) for dNTP and nucleotide analogues lacking the 3′-OH. If these two mutants have lost the capability to interact with the 3′-OH of dTTP, the binding of the nucleotide analogues lacking the 3′-OH to the active sites of these mutants should not be affected by these two mutations. In this study, we tested this prediction by employing the two HIV-1 RT mutants and the natural dTTP substrate, as well as three different nucleotide analogues, ddTTP, acyTTP, and AZTTP, containing various modifications at the 3′ position of their sugar moiety. As observed in Tables 1 and 2, unlike wild-type HIV-1 RT, these two RT mutants showed slightly decreased but comparable binding affinities to ddTTP compared to dTTP. Furthermore, no K_d difference between wild-type and mutant RTs was also observed for ddTTP and acyTTP, which is also consistent with our structure-based predictions. Therefore, the kinetic data corroborate a structural model for the direct hydrogen bond mediated interaction between the side chain of Q151 and the 3′-OH of dTTP in the solution state.

It is not clear whether the other three kinds of dNTP (i.e., dATP, dCTP, and dGTP) substrates form exactly the same molecular interactions with active site residues as dTTP does. In addition, the interaction of HIV-1 RT with dNTP substrates may vary in the complex formed with template-primer with different properties (sequences and RNA versus DNA template). This possibility is supported by the kinetic variations observed with different substrates (T/P and dNTPs). For example, the reported K_d values of wild-type HIV-1 RT with dTTP and dCTP vary significantly, ranging from 1.5 μM (DNA template) to 28 μM (RNA template) (*32*) and 7.88 μM (DNA template) to 30 μM (RNA template), respectively (*10*, *11*), suggesting that the quality of the interactions between dNTP and the RT active site residues also changes during the DNA synthesis from heteropolymeric viral genomic sequences. Is the Q151 residue important in the binding of every dNTP in T/Ps containing heteropolymeric sequences? The possibility that the requirement of the Q151−3′-OH interaction may vary is supported by previous studies reporting different K_d values representing ratios between dNTP and ddNTPs. For example, it was reported that the K_d values of wild-type HIV-1 RT with ddATP and ddCTP are 5- and 2-fold higher than those with dATP and dCTP, respectively (*10*). Our preliminary data also showed that K_d value differences between dATP and ddATP are less obvious, compared to K_d value differences between dTTP and ddTTP (14-fold). Other studies with different T/Ps also have reported minor K_d differences between dATP and ddATP (*12*). These findings indicate that the significance of the Q151 residue interaction with the 3′-OH of dNTP varies, depending on the nucleotide substrates and the nature of the T/Ps used. Structural analysis on the HIV-1 RT complex with different dNTPs can confirm whether the variation in the Q151−3′-OH interaction occurs among the ternary complex formed with various dNTPs. Studies with thermostable *Taq* polymerase have demonstrated widely different incorporation efficiencies among ddNTPs (*2*). Structural analysis on four different closed complexes with each ddNTP revealed distinct structural variations among the complexes with different ddNTPs. Modeling in this study suggested that preferential incorporation of ddGTP by *Taq* polymerase could result from a unique hydrogen bond interaction between the side chain of Arg660 and O6/N7 of ddGTP (*1*).

The incorporation of acyCTP (as well as ddCTP and dCTP) by thermostable Vent DNA polymerase has been studied (*8*). Vent polymerase discriminates dCTP and ddCTP exclusively in the k_{pol} step. Interestingly, even though the binding affinities of Vent polymerase for acyCTP and ddCTP, as well as dCTP, are very similar, this polymerase incorporates acyCTP 28 times more efficiently than ddCTP by facilitating the phosphoryl transfer rate. However, its k_{pol} value for acyCTP is still 8 times lower than that for dCTP. As shown in Tables 1 and 2, wild-type HIV-1 RT uses both K_d and k_{pol} steps to differentiate acyTTP over ddTTP. Interestingly, unlike Vent polymerase wild-type HIV-1 RT has 4-fold lower binding affinity for acyTTP than for ddTTP. In contrast, like Vent polymerase, wild-type HIV-1 RT showed 5 times higher k_{pol} values for acyTTP than ddTTP (Table 2). This leads to the similar incorporation efficiency (k_{pol}/K_d) of wild-type HIV-1 RT for acyTTP and ddTTP (Tables 1 and 2), which is different from Vent polymerase that prefers incorporation of acyNTPs over ddNTPs. Basically, while Vent DNA polymerase can differentiate the chemical modification difference between ddNTP and acyNTPs during the k_{pol} step, the active site of HIV-1 RT

differentiates acyTTP and ddTTP in both K_d and k_{pol} steps, but in opposite ways. In addition, due to relatively high k_{pol} values with acyCTP, Vent polymerase has only 10-fold lower incorporation efficiency (k_{pol}/K_d) for acyCTP than dCTP, even though this polymerase has 270-fold reduced incorporation efficiency (k_{pol}/K_d) for ddCTP, compared to dCTP. However, wild-type HIV-1 RT has 103- and 69-fold lower incorporation efficiency for ddTTP and acyTTP, respectively, compared to dTTP.

One interesting observation in our study was that the two Q151N and V148I mutants had tighter binding affinity to AZTTP, compared to ddTTP and acyTTP. In fact, these two mutants had tighter binding affinity to AZTTP than even the natural dTTP substrate. The original crystallographic analysis of AZTTP proposed that N4 and N6 of the azido group on AZTTP can form two hydrogen bonds by accepting protons possibly donated from the RT active site residues, which explains tight binding of AZTTP to HIV-1 RT (similar K_d with dTTP) (*33*). The length between N4 and N6 is 2.35 Å, and the total length of the azido group from the C3′ of the AZTTP becomes 3.82 Å, which is 1.43 Å longer than that of the OH group of dTTP (2.39 Å). One possible model for the tight binding affinity of wild-type HIV-1 RT to AZTTP is that the N4 of the azido group may interact with the amide side chain of the wild-type Q151. A second hydrogen bond between the N6 azido atom and the amide hydrogens of F116 of the short helix could form as well. The dipole of this helix could be a stabilizing factor that accounts for the tighter binding to AZTTP. In contrast, even though the shortened side chain of the N151 mutant residue appears to preclude contact with the 3′-OH of dTTP, the N151 mutant side chain may be able to make some contact with the azido group of AZTTP, which is 1.43 Å longer than the 3′-OH of dTTP, leading to the tighter binding affinity of the Q151N mutant to AZTTP, compared to dTTP (Figure 6). Most likely, the shortened side chain of the N151 mutant forms one hydrogen bond possibly at N4 or N6 as a consequence of the need to make space for the long azido group of AZTTP.

Interestingly, an in vivo mutation, Q151M, has been identified among AZT-resistant RT variants, and this mutation is often identified transiently during AZT treatment (*34*). Pre-steady-state kinetic analysis of the Q151M single mutant RT revealed 2.5-fold K_d or reduced binding affinity for AZTTP compared to wild-type RT, supporting a model for the direct interaction between the azido group of AZT and the Q151 residue of HIV-1 RT (*34*). This mutant also showed 3-fold reduced k_{pol} with AZTTP relative to WT RT. Therefore, the Q151M mutant reduces the AZTMP incorporation efficiency (k_{pol}/K_d) by 7.5-fold using both k_{pol} and K_d steps. As shown in Table 2, the Q151N mutant also reduces the binding affinity (5-fold) to AZTTP. However, in contrast to the Q151M, the k_{pol} value of the Q151N mutant is actually slightly higher (1.8-fold) than wild-type RT, resulting in only a 2.8-fold decrease in the AZTMP incorporation efficiency (k_{pol}/K_d). This minimal effect of the AZT incorporation, together with a large defect in the dTTP incorporation efficiency (i.e., low K_d), could restrict the selection of the Q151N mutation as an AZT- resistant mutation. Unlike the Q151N mutant, the Q151M AZT-resistant mutation has wild-type levels of K_d and k_{pol} for dTTP. We recently showed that the Q151N mutant RT virus

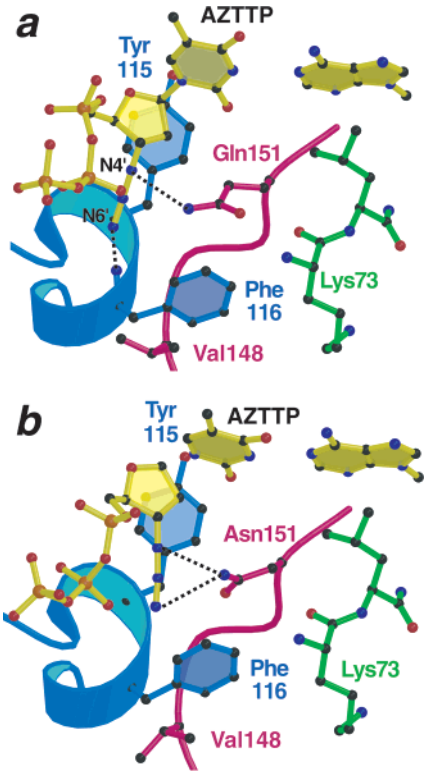

FIGURE 6: Structural models for the active sites of wild-type and Q151N mutant HIV-1 RT interacting with AZTTP. (a) The native RT active site showing Gln151 interacting with AZTTP (ball-and-stick model) via a hydrogen bond between the amide moiety and the N4′ position of the nucleotide analogue. The additional methylene group of the Gln151 side chain pushes the AZTTP nucleotide away from the red loop such that the azido moiety is positioned over a helix dipole. A second hydrogen bond may form between the N6′ position of AZTTP and the backbone amide hydrogen of Phe116, which resides in the small helical segment located in the floor of the active site cavity. (b) The Q151N mutant forms potential hydrogen bonds to the N4′ and N6′ atoms of AZTTP but does not experience the crowding observed for Gln151.

(and the V148I RT virus) failed to infect macrophage containing low cellular dNTP concentrations (~40 nM) even though the mutant viruses were able to infect activated T cells containing high dNTP concentrations (2−5 μM). High K_d values of these mutant RTs, which reduced their capability to synthesize DNA at low dNTP concentrations, likely contribute to the restricted infection of the Q151N (and V148I) mutant virus to nondividing macrophage. However, since the Q151M RT has wild-type kinetic properties, the Q151M mutation should not affect viral infectivity significantly and can be selected as an in vivo AZT-resistant mutation.

In this study, we presented kinetic evidence supporting the interaction between the side chain of the Q151 residue of HIV-1 RT and the 3′-OH of the incoming dTTP, which was observed in the crystal structure of the ternary complex of HIV-1 RT with dTTP. This study also provided mechanistic insights into the possible interaction between the active site of HIV-1 RT and chemically modified groups at the 3′ position of NRTIs.

ACKNOWLEDGMENT

We thank Dr. Mini Balakrishnan for critical reading of the manuscript.

REFERENCES

1. Ying, L., Vesselin, M., and Gabriel, W. (1999) Structure-based design of Taq DNA polymerase with improved properties of dideoxynucleotide incorporation, *Biochemistry 96*, 9491−9496.
2. Brandis, J. W., Sydney, G. E., and Johnson, K. A. (1996) Slow rate of phosphodiester bond formation accounts for the strong bias that Taq DNA polymerase shows against 2′,3′-dideoxynucleotide terminators, *Biochemistry 35*, 2189−2200.
3. Cohen, S. S. (1977) The mechanisms of lethal action of arabinosyl cytosine (ara C) and arabinosyl adenine (ara A), *Cancer 40*, 509−518.
4. Hiddemann, W. (1991) Cytosine arabinoside in the treatment of acute myeloid leukemia: the role and place of high-dose regimens, *Ann. Hematol. 62*, 119−128.
5. Ray, A. S., Yang, Z., Shi, J., Hobbs, A., Schinazi, R. F., Chu, C. K., and Anderson, K. S. (2002) Insights into the molecular mechanism of inhibition and drug resistance for HIV-1RT with carbovir triphosphate, *Biochemistry 41*, 5150−5162.
6. Nikoenko, G. N., Palmer, S., Maldarelli, F., Mellors, J. W., Coffin, J. M., and Pathak, V. K. (2005) Mechanism for nucleoside analog-mediated abrogation of HIV-1 replication: balance between RNase H activity and nucleoside excision, *Proc. Natl. Acad. Sci. U.S.A. 102*, 2093−2098.
7. Astatke, M., Grindley, N. D. F., and Joyce, C. M. (1998) How *E. coli* DNA polymerase I (Klenow fragment) distinguishes between deoxy- and dideoxynucleotides, *J. Mol. Biol. 278*, 147−165.
8. Gardner, A. F., Joyce, C. M., and Jack, W. E. (2004) Comparative kinetics of nucleotide analog incorporation by Vent DNA polymerase, *J. Biol. Chem. 279*, 11834−11842.
9. Yang, G., Franklin, M., Li, J., Lin, T. C., and Konigsberg, W. (2002) A conserved Tyr residue is required for sugar selectivity in a Pol a DNA polymerase, *Biochemistry 41*, 10256−10261.
10. Selmi, B., Boretto, J., Sarfati, S. R., Guerreiro, C., and Canard, B. (2001) Mechanism-based suppression of dideoxynucleotide resistance by K65R human immunodeficiency virus reverse transcriptase using an α-boranophosphate nucleoside analogue, *J. Biol. Chem. 276*, 48466−48472.
11. Feng, J. Y., and Anderson, K. S. (1999) Mechanistic studies comparing the incorporation of (+) and (−) isomers of 3TCTP by HIV-1 reverse transcriptase, *Biochemistry 38*, 55−63.
12. Deval, J., Navarro, J., Selmi, B., Courcambeck, J., Boretto, J., Halfon, P., Garrido-Urbani, S., Sire, J., and Canard, B. (2004) A loss of viral replicative capacity correlates with altered DNA polymerization kinetics by the human immunodeficiency virus reverse transcriptase bearing the K65R and L74V dideoxynucleoside resistance substituions, *J. Biol. Chem. 279*, 25489−25496.
13. Suo, Z., and Johnson, K. A. (1998) Selective inhibition of HIV-1 reverse transcriptase by an antiviral inhibitor, (R)-9-(2-phosphonylmethoxypropyl) adenine, *J. Biol. Chem. 273*, 27250−27258.
14. Feng, J. Y., Murakami, E., Zorca, S. M., Johnson, A. A., Johnson, K. A., Schinazi, R. F., Furman, P. A., and Anderson, K. S. (2004) Relationship between antiviral activity and host toxicity comparison of the incorporation efficiencies of 2′,3′-dideoxy-5-fluoro-3′-thiacytidine-triphosphate analogs by human immunodeficiency virus type-1 reverse transcriptase and human mitochondrial DNA polymerase, *Antimicrob. Agents Chemother. 48*, 1300−1306.
15. Huang, H., Chopra, R., Verdine, G. L., and Harrison, S. C. (1998) Structure of a covalently trapped catalytic complex of HIV-1 reverse transcriptase: implications for drug resistance, *Science 282*, 1669−1675.
16. Weiss, K. K., Chen, R., Skasko, M., Reynolds, H. M., Lee, K., Bambara, R. A., Mansky, L. M., and Kim, B. (2004) A role for dNTP binding of human immunodeficiency virus type 1 reverse transcriptase in viral mutagenesis, *Biochemistry 43*, 4490−4500.
17. Weiss, K. K., Bambara, R. A., and Kim, B. (2002) Mechanistic role of residue Gln151 in error prone DNA synthesis by human immunodeficiency virus type 1 (HIV-1) reverse transcriptase (RT). Pre-steady-state kinetic study of the Q151N HIV-1 RT mutant with increased fidelity, *J. Biol. Chem. 277*, 22662−22669.
18. Diamond, T. L., Kimata, J., and Kim, B. (2001) Identification of a simian immunodeficiency virus reverse transcriptase variant with enhanced replicational fidelity in the late stage of viral infection, *J. Biol. Chem. 276*, 23624−23631.
19. Diamond, T. L., Souroullas, G., Weiss, K. K., Lee, K. Y., Bambara, R. A., Dewhurst, S., and Kim, B. (2003) Mechanistic understanding of an altered fidelity simian immunodeficiency virus reverse transcriptase mutation, V148I, identified in a pig-tailed macaque, *J. Biol. Chem. 278*, 29913−29924.
20. Diamond, T. L., Roshal, M., Jamburuthugoda, V. K., Reynolds, H. M., Merriam, A. R., Lee, K. Y., Balakrishnan, M., Bambara, R. A., Planelles, V., Dewhurst, S., and Kim, B. (2004) Macrophage tropism of HIV-1 depends upon efficient cellular dNTP utilization by reverse transcriptase, *J. Biol. Chem. 279*, 51545−51553.
21. Weiss, K. K., Isaacs, S. J., Tran, N. H., Adman, E. T., and Kim, B. (2000) Molecular architecture of the mutagenic active site of human immunodeficiency virus type 1 reverse transcriptase: roles of the beta 8-alpha E loop in fidelity, processivity, and substrate interactions, *Biochemistry 39*, 10684−10694.
22. Malboeuf, C. M., Isaacs, S. J., Tran, N. H., and Kim, B. (2001) Thermal effects on reverse transcription: improvement of accuracy and processivity in cDNA synthesis, *BioTechniques 30*, 1074−1078, 1080, 1082, passim.
23. Kim, B. (1997) Genetic selection in *Escherichia coli* for active human immunodeficiency virus reverse transcriptase mutants, *Methods 12*, 318−324.
24. Jones, T. A., Zou, J. Y., Cowan, S. W., and Kjeldgaard (1991) Improved methods for building protein models in electron density maps and the location of errors in these models, *Acta Crystallogr. A47*, 110−119.
25. Brünger, A. T., Adams, P. D., Clore, G. M., DeLano, W. L., Gros, P., Grosse-Kunstleve, R. W., Jiang, J. S., Kuszewski, J., Nilges, M., Pannu, N. S., Read, R. J., Rice, L. M., Simonson, T., and Warren, G. L. (1998) Crystallography & NMR system: A new software suite for macromolecular structure determination, *Acta Crystallogr. D54*, 905−921.
26. Johnson, K. A. (1995) Rapid quench kinetic analysis of polymerases, adenosinetriphosphatases, and enzyme intermediates, *Methods Enzymol. 249*, 38−61.
27. Kati, W. M., Johnson, K. A., Jerva, L. F., and Anderson, K. S. (1992) Mechanism and fidelity of HIV reverse transcriptase, *J. Biol. Chem. 267*, 25988−25997.
28. Johnson, K. A. (1993) Conformational coupling in DNA polymerase fidelity, *Annu. Rev. Biochem. 62*, 685−713.
29. Kerr, S. G., and Anderson, K. S. (1997) Pre-steady-state kinetic characterization of wild type and 3′-azido-3′-deoxythymidine (AZT) resistant human immunodeficiency virus type 1 reverse transcriptase: implication of RNA directed DNA polymerization in the mechanism of AZT resistance, *Biochemistry 36*, 14064−14070.
30. Feng, J. Y., and Anderson, K. S. (1999) Mechanistic studies examining the efficiency and fidelity of DNA synthesis by the 3TC-resistant mutant (184V) of HIV-1 reverse transcriptase, *Biochemistry 38*, 9440−9448.
31. Reardon, J. E. (1993) Human immunodeficiency virus reverse transcriptase: A kinetic analysis of RNA-dependent and DNA-dependent DNA polymerization, *J. Biol. Chem. 268*, 8743−8751.
32. Vaccaro, J. A., Parnell, K. M., Terezakis, S. A., and Anderson, K. S. (2000) Mechanism of inhibition of the human immunodeficiency virus type 1 reverse transcriptase by d4TTP: an equivalent incorporation efficiency relative to the natural substrate dTTP, *Antimicrob. Agents Chemother. 44*, 217−221.
33. Camerman, A., Mastropaolo, D., and Camerman, N. (1987) Azidothymidine: crystal structure and possible functional role of the azido group, *Proc. Natl. Acad. Sci. U.S.A. 84*, 8239−8242.
34. Deval, J., Selmi, B., Boretto, J., Egloff, M. P., Guerreiro, C., Sarfati, S., and Canard, B. (2002) The molecular mechanism of multidrug resistance by the Q151M human immunodeficiency virus type 1 reverse transcriptase and its suppression using α-boranophosphate nucleotide analogues, *J. Biol. Chem. 277*, 42097−42104.
35. Skasko, M., Weiss, K. K., Reynolds, H. M., Jamburuthugoda, V., Lee, K., and Kim, B. (2005) Mechanistic differences in RNA dependent DNA polymerization and fidelity between murine leukemia virus and human immunodeficiency virus type 1 reverse transcriptases, *J. Biol. Chem. 280*, 12190−12200.

BI050611+